Supplementary Information

Convection-Enhanced Delivery *in silico* study for personalized brain cancer treatment

Chryso Lambride, Vasileios Vavourakis, Triantafyllos Stylianopoulos

The reflection coefficient (see Equation (5) in the manuscript) is defined through: $\sigma_f = 1 - W$, where H and W correspond to the hydrodynamic coefficients for neutral spheres in cylindrical pores: $H = 6\,\pi\,F/K_t$ and $W = F\,(2-F)\,K_s/K_t$; with F being the partition coefficient: $F = (1-\lambda)^2$, and λ the ratio of the drug (effective) size to the vessel wall pore (effective) size. Coefficients K_t and K_s are calculated, $\binom{K_t}{K_s} = \frac{9}{4}\pi^2\sqrt{2}(1-\lambda)^{-5/2} + \left[1 + \sum_{n=1}^{2}\binom{a_n}{b_n}(1-\lambda)^n\right] + \sum_{n=0}^{4}\binom{a_{n+3}}{b_{n+3}}\lambda^n$, where a and b are constant parameters listed in the Supplementary Table S1.

Supplementary Table S1: Constant Coefficients a and b for determining coefficients K_t and K_s, respectively[1].

Constant Coefficient - a	Value	Constant Coefficient - b	Value
a_1	−1.217	b_1	0.117
a_2	1.534	b_2	−0.044
a_3	−22.508	b_3	4.018
a_4	−5.617	b_4	−3.979
a_5	−0.336	b_5	−1.922
a_6	−1.216	b_6	4.392
a_7	1.647	b_7	5.006

Supplementary Table S2: Values of all FE model parameters used in the CED brain simulations**.**

Parameter	Description	Domain	Value	Reference
r_s	Drug radius	-	0.5, 10, 30 nm	[2,3]
r_o	Vascular wall pore radius	Normal tissue	3.5 nm	[4-6]
		Tumor tissue	25, 50, 75 nm	
D_i	Drug diffusion coefficient	All tissues	5.82×10^{-10} m²/s for 0.5nm drug radius, 9.28×10^{-12} m²/s for 10nm drug radius, 3.28×10^{-12} m²/s for 30nm drug radius	[7]
k	Hydraulic conductivity of tissue interstitial space	Gray Matter	2×10^{-14} $m^2(Pa\cdot s)^{-1}$	[8-10]
		White Matter	2×10^{-13} $m^2(Pa\cdot s)^{-1}$	
		Tumor tissue	2×10^{-14} $m^2(Pa\cdot s)^{-1}$ 2×10^{-13} $m^2(Pa\cdot s)^{-1}$ 2×10^{-13} $m^2(Pa\cdot s)^{-1}$	
S_v	Vascular density of blood vessels	Normal tissue	70 $(cm)^{-1}$	[11,12]
		Tumor tissue	50 $(cm)^{-1}$	
$L_{pl}S_{vl}$	Permeability of Lymphatics	Normal tissue	2.24×10^{-11} m²·s/kg	[13,14]
		Tumor tissue	0	
γ	Fraction of vessel wall surface area occupied by pores	All tissues	1×10^{-3}	[11]
C_v	Vascular drug concentration	All tissues	0	-
p_v	Vascular pressure of blood vessels	All tissues	2.0 kPa	[14]
p_l	Vascular pressure of lymphatic vessels	All tissues	0.0 kPa	[15]
L_{vw}	Vessel wall thickness	All tissues	5×10^{-6} m	[16]
T	Temperature	All tissues	310 K	[11]
μ	Interstitial fluid viscosity	All tissues	7.8×10^{-4} Pa·s	[17,18]
	Plasma viscosity	-	1.30×10^{-3} Pa·s	
ρ	Interstitial fluid density	All tissues	1000 kg/m³	[17]
ε_p	Tissue porosity	All tissues	0.3	[19]
k_d	Drug degradation constant	All tissues	2×10^{-5} s^{-1}	[19]
k_l	Lymphatic drainage constant	Normal tissue	1×10^{-4} s^{-1}	[20]

*Normal tissue includes grey and white matter of the brain.

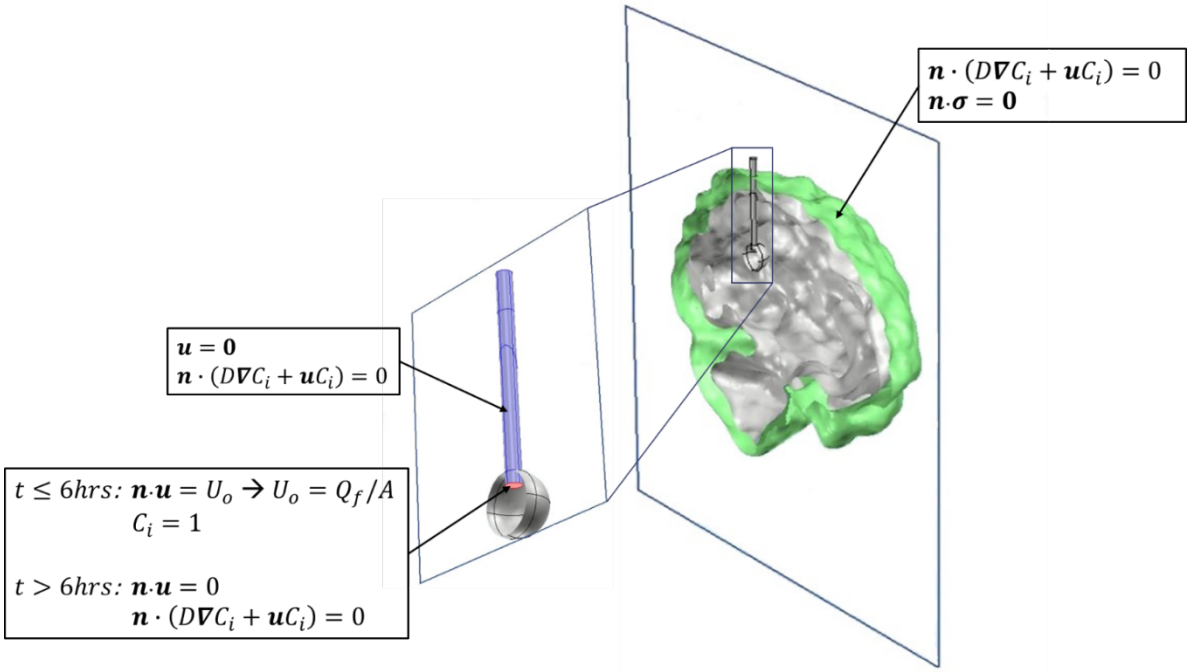

Supplementary Figure S1. Boundary conditions of the 3D model. At the interface between the catheter and tumor the normal inlet velocity (*i.e.,* $U_o=Q_f/A$, A cross section of the catheter) was taken equal to 1.99×10^{-5}m/s and infusion lasted for 6 hours. Also, at the interface of the catheter and tumor tissue, the relative drug concertation was set to unity for the period of the infusion and after completion of infusion, a zero-flux boundary condition was applied (*i.e.*, $\boldsymbol{n}\cdot(D\boldsymbol{\nabla}C_i\text{-}C_i\boldsymbol{u})=0$, where $\boldsymbol{n}$ corresponds to the outward unit normal vector).The normal stresses on the outer brain surfaces were equal to zero (*i.e.*, $\boldsymbol{n}\cdot\boldsymbol{\sigma}=\boldsymbol{0}$). At the catheter surfaces, a no-slip boundary condition was applied for fluid velocity (*i.e.*, $\boldsymbol{u}=\boldsymbol{0}$) and additionally, a zero-flux boundary condition was set for the transport of the drugs. The latter boundary condition was also set at the outer brain surfaces.

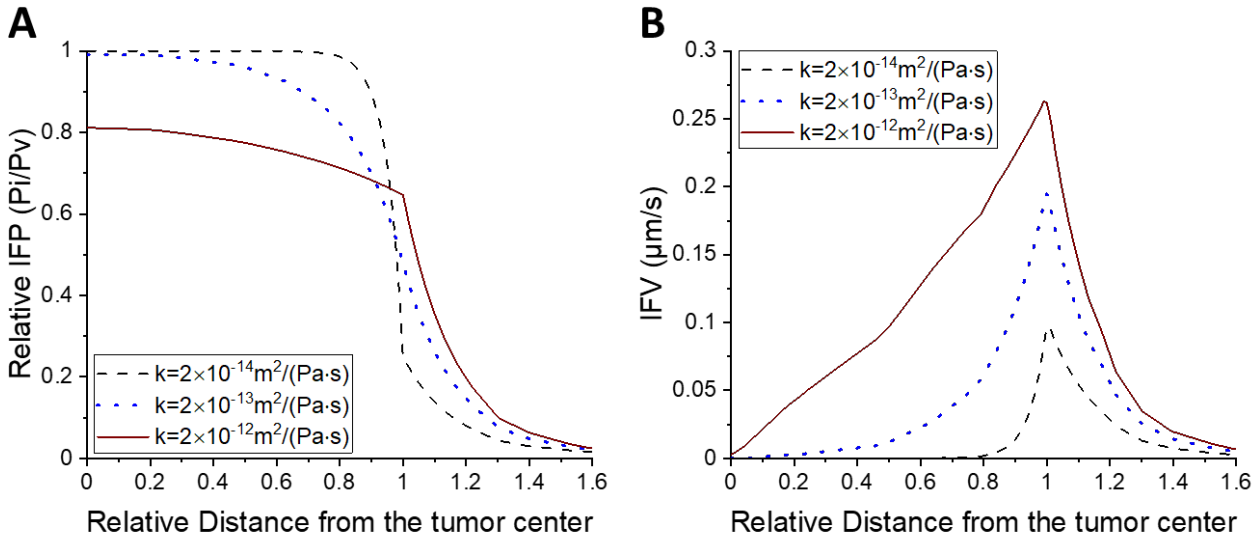

Supplementary Figure S2. IFP and IFV as a function of the distance from the tumor center for baseline value of the vessel wall pore diameter. IFP and IFV as a function of the distance from the tumor center for different hydraulic conductivities of the tumor interstitial space and 100 nm diameter of vascular wall pores. *In silico* predicted (A) relative fluid pressure (p_i/p_v) and (B) velocity magnitude of the tumor interstitial space before CED administration. IFP is normalized by division with the vascular pressure of blood vessels, p_v. Distance is normalized by division with the tumor radius.

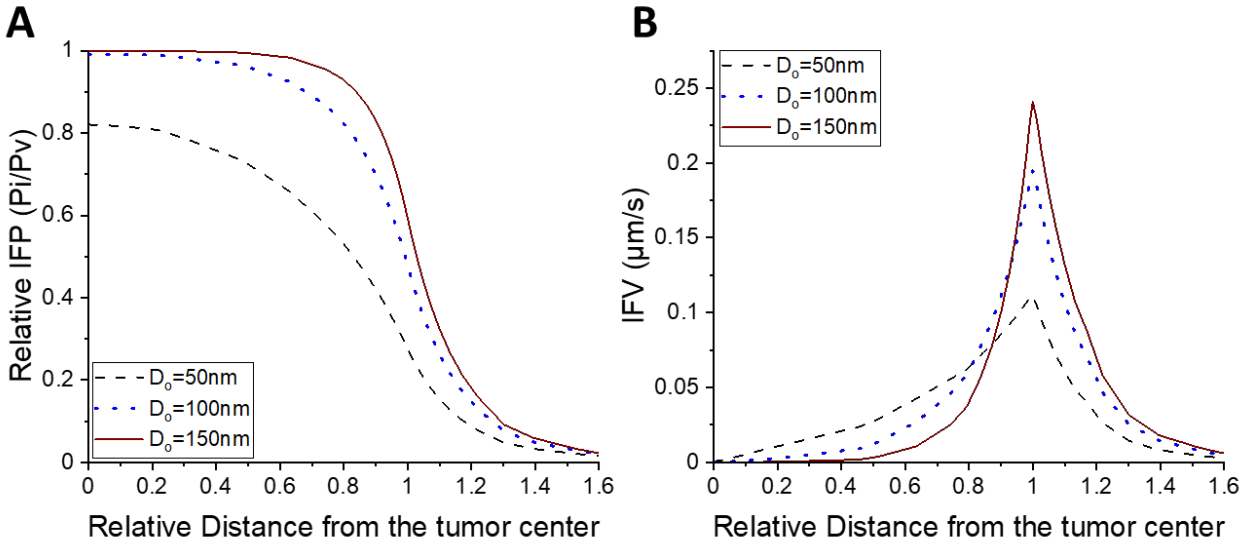

Supplementary Figure S3. IFP and IFV as a function of the distance from the tumor center for baseline value of hydraulic conductivity of the tumor interstitial space. IFP and IFV as a function of the distance from the tumor center for different diameters of vascular wall pores and 2×10^{-13} $m^2(Pa\cdot s)^{-1}$ hydraulic conductivity of the tumor interstitial space. *In silico* predicted (A) relative fluid pressure (p_i/p_v) and (B) velocity magnitude of the tumor interstitial space before CED administration. IFP is normalized by division with the vascular pressure of blood vessels, p_v. Distance is normalized by division with the tumor radius.

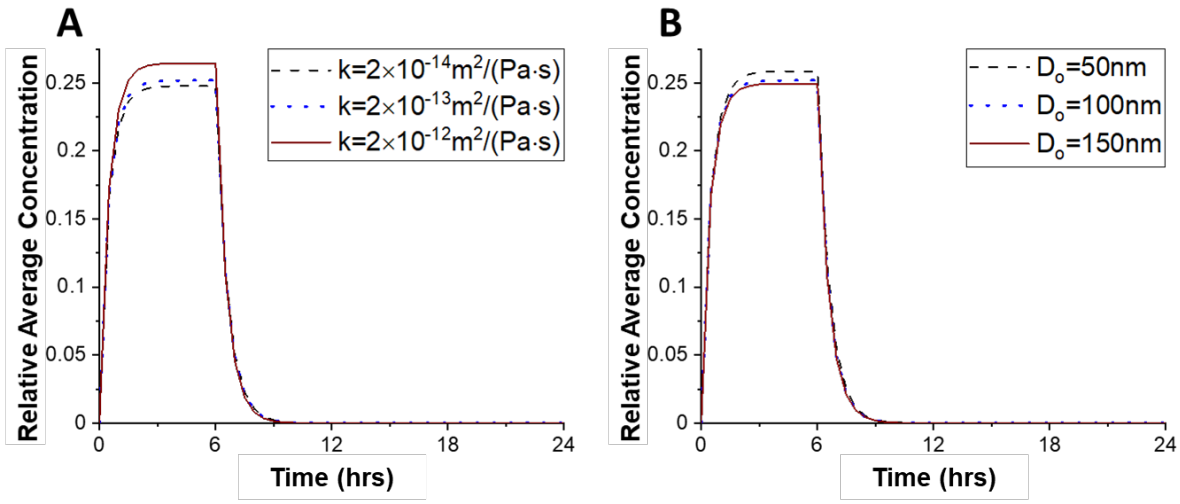

Supplementary Figure S4. Average concentration in tumor tissue as a function of time for 1 nm diameter of the therapeutic agent. *In silico* predicted average relative concentration: (A) different hydraulic conductivities of the tumor interstitial space and 100 nm diameter of vascular wall pores and (B) different diameters of vascular wall pores and 2×10^{-13} $m^2(Pa\cdot s)^{-1}$ hydraulic conductivity of the tumor interstitial space. Drug concentration is normalized by division with the reference value entering the catheter.

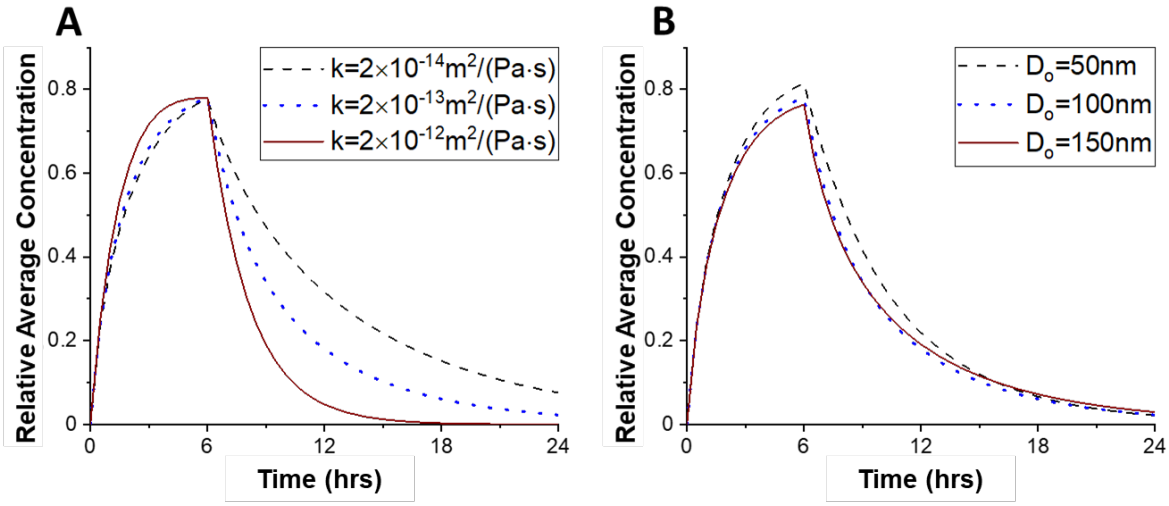

Supplementary Figure S5. Average concentration in tumor tissue as a function of the time for 20 nm diameter of the therapeutic agent. *In silico* predicted average relative concentration: (A) different hydraulic conductivities of the tumor interstitial space and 100nm diameter of vascular wall pores and (B) different diameters of vascular wall pores and $2\times10^{-13}m^2(Pa\cdot s)^{-1}$ hydraulic conductivity of the tumor interstitial space. Drug concentration is normalized by division with the reference value entering the catheter.

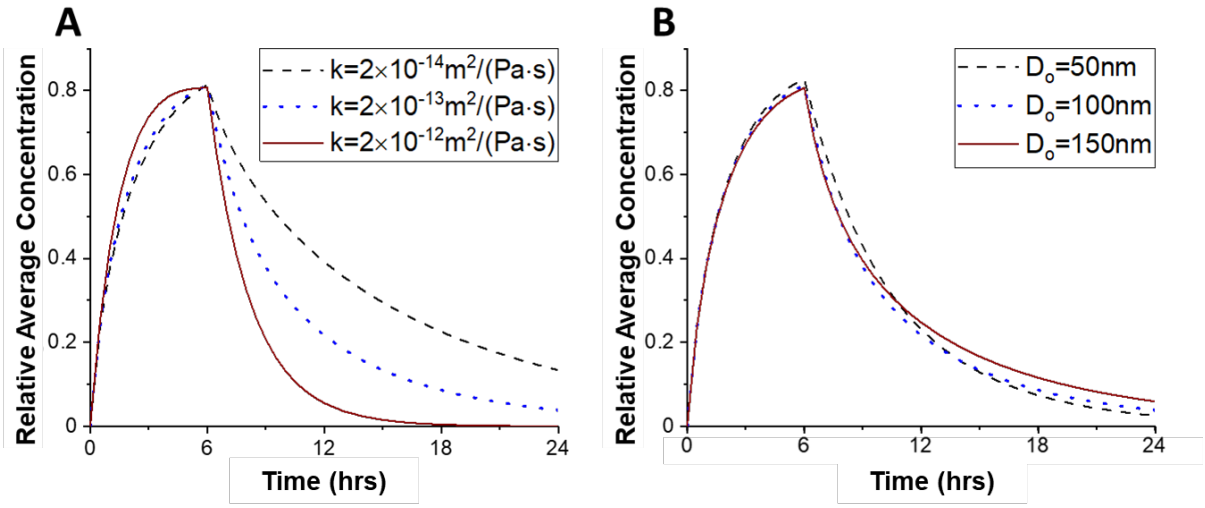

Supplementary Figure S6. Average concentration in tumor tissue as a function of the time for 60 nm diameter of the therapeutic agent. *In silico* predicted average relative concentration: (A) different hydraulic conductivities of the tumor interstitial space and 100nm diameter of vascular wall pores and (B) different diameters of vascular wall pores and $2\times10^{-13}\,m^2(Pa\cdot s)^{-1}$ hydraulic conductivity of the tumor interstitial space. Drug concentration is normalized by division with the reference value entering the catheter.

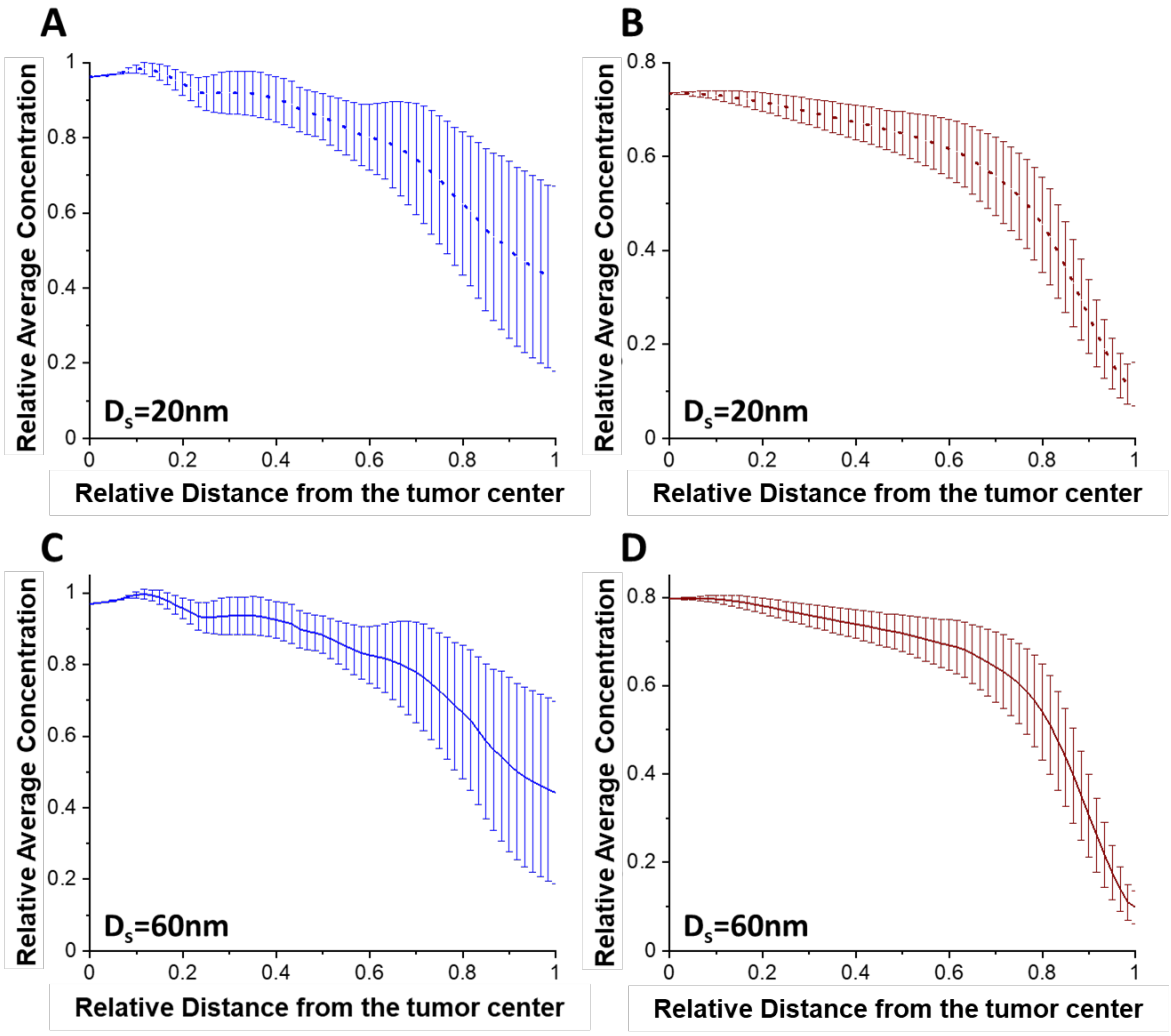

Supplementary Figure S7. Average drug concentration as a function of the distance from the tumor center plots for the lowest hydraulic conductivity of the tumor interstitial space. Average relative concentration calculated along the four directions as a function of the relative distance from the tumor center (A, C) after 5 hrs and (B, D) after 9 hrs, for 2×10^{-14} $m^2(Pa\cdot s)^{-1}$ hydraulic conductivity of the tumor interstitial space, 100 nm different pore diameter of tumor vascular walls, and for different drug diameters: (A, B) 20 nm and (C, D) 60 nm. Drug concentration is normalized by division with the reference value entering the catheter. Distance is normalized by division with the tumor radius.

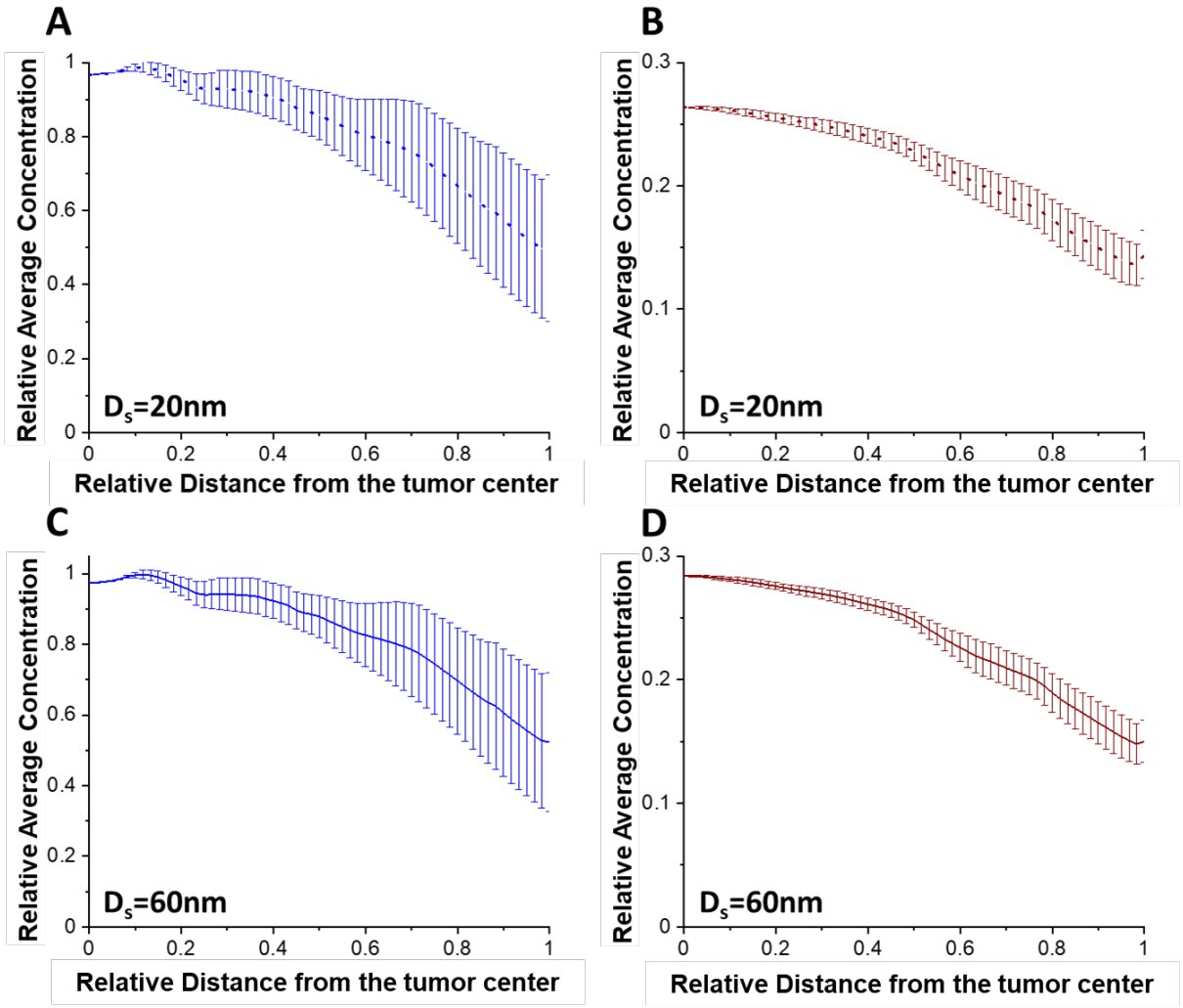

Supplementary Figure S8. Average drug concentration as a function of the distance from the tumor center plots for the highest hydraulic conductivity of the tumor interstitial space. Average relative concentration calculated along the four directions as a function of the relative distance from the tumor center (A, C) after 5 hrs and (B, D) after 9 hrs, for 2×10^{-12} $m^2(Pa\cdot s)^{-1}$ hydraulic conductivity of the tumor interstitial space, 100nm different pore diameter of tumor vascular walls, and for different drug diameters: (A, B) 20 nm and (C, D) 60 nm. Drug concentration is normalized by division with the reference value entering the catheter. Distance is normalized by division with the tumor radius.

References

1 Deen, W. M. Hindered Transport of Large molecules in Liquid-Filled Pores. *AIChE J* **33**, 1409-1425 (1987).

2 Koo, Y.-E. L. *et al.* Brain cancer diagnosis and therapy with nanoplatforms. *Advanced drug delivery reviews* **58**, 1556-1577 (2006).

3 Allard, E., Passirani, C. & Benoit, J. P. Convection-enhanced delivery of nanocarriers for the treatment of brain tumors. *Biomaterials* **30**, 2302-2318, doi:10.1016/j.biomaterials.2009.01.003 (2009).

4 Hobbs, S. K. *et al.* Regulation of transport pathways in tumor vessels: role of tumor type and microenvironment. *Proceedings of the National Academy of Sciences of the United States of America* **95**, 4607-4612 (1998).

5 Sarin, H. *et al.* Physiologic upper limit of pore size in the blood-tumor barrier of malignant solid tumors. *Journal of translational medicine* **7**, 51, doi:10.1186/1479-5876-7-51 (2009).

6 Wang, J., Lu, Z., Gao, Y., Wientjes, M. G. & Au, J. L. Improving delivery and efficacy of nanomedicines in solid tumors: role of tumor priming. *Nanomedicine* **6**, 1605-1620, doi:10.2217/nnm.11.141 (2011).

7 Pluen, A. *et al.* Role of tumor-host interactions in interstitial diffusion of macromolecules: cranial vs. subcutaneous tumors. *Proceedings of the National Academy of Sciences of the United States of America* **98**, 4628-4633, doi:10.1073/pnas.081626898 081626898 [pii] (2001).

8 Netti, P. A., Berk, D. A., Swartz, M. A., Grodzinsky, A. J. & Jain, R. K. Role of extracellular matrix assembly in interstitial transport in solid tumors. *Cancer research* **60**, 2497-2503 (2000).

9 Angeli, S. & Stylianopoulos, T. Biphasic modeling of brain tumor biomechanics and response to radiation treatment. *Journal of biomechanics*, doi:10.1016/j.jbiomech.2016.03.029 (2016).

10 Smith, J. H. & Humphrey, J. A. Interstitial transport and transvascular fluid exchange during infusion into brain and tumor tissue. *Microvascular research* **73**, 58-73, doi:10.1016/j.mvr.2006.07.001 (2007).

11 Mpekris, F., Baish, J. W., Stylianopoulos, T. & Jain, R. K. Role of vascular normalization in benefit from metronomic chemotherapy. *Proceedings of the National Academy of Sciences of the United States of America* **114**, 1994-1999, doi:10.1073/pnas.1700340114 (2017).

12 Jain, R. K., Tong, R. T. & Munn, L. L. Effect of vascular normalization by antiangiogenic therapy on interstitial hypertension, peritumor edema, and lymphatic metastasis: insights from a mathematical model. *Cancer research* **67**, 2729-2735, doi:67/6/2729 [pii] 10.1158/0008-5472.CAN-06-4102 (2007).

13 Scallan, J. P. & Huxley, V. H. In vivo determination of collecting lymphatic vessel permeability to albumin: a role for lymphatics in exchange. *The Journal of physiology* **588**, 243-254, doi:10.1113/jphysiol.2009.179622 (2010).

14 Stylianopoulos, T., Munn, L. L. & Jain, R. K. Reengineering the Physical Microenvironment of Tumors to Improve Drug Delivery and Efficacy: From Mathematical Modeling to Bench to Bedside. *Trends Cancer* **4**, 292-319, doi:10.1016/j.trecan.2018.02.005 (2018).

15 Voutouri, C. & Stylianopoulos, T. Evolution of osmotic pressure in solid tumors. *Journal of biomechanics* **47**, 3441-3447, doi:10.1016/j.jbiomech.2014.09.019 (2014).

16 Stylianopoulos, T. *et al.* Coevolution of solid stress and interstitial fluid pressure in tumors during progression: Implications for vascular collapse. *Cancer research* **73**, 3833-3841, doi:10.1158/0008-5472.can-12-4521 (2013).

17 Zhan, W. & Wang, C. H. Convection enhanced delivery of liposome encapsulated doxorubicin for brain tumour therapy. *Journal of controlled release : official journal of the Controlled Release Society* **285**, 212-229, doi:10.1016/j.jconrel.2018.07.006 (2018).

18 Kesmarky, G., Kenyeres, P., Rabai, M. & Toth, K. Plasma viscosity: a forgotten variable. *Clinical hemorheology and microcirculation* **39**, 243-246 (2008).

19 Linninger, A. A., Somayaji, M. R., Mekarski, M. & Zhang, L. Prediction of convection-enhanced drug delivery to the human brain. *Journal of theoretical biology* **250**, 125-138, doi:10.1016/j.jtbi.2007.09.009 (2008).

20 Zhan, W., Alamer, M. & Xu, X. Y. Computational modelling of drug delivery to solid tumour: Understanding the interplay between chemotherapeutics and biological system for optimised delivery systems. *Adv Drug Deliv Rev* **132**, 81-103, doi:10.1016/j.addr.2018.07.013 (2018).